Original Paper

Indoor and Built Environment

Indoor and Built Environment
0(0) 1–14

DOI: 10.1177/1420326X16635260
ibe.sagepub.com

SAGE

Simulation of indoor comfort level in a building cooled by a cooling tower–concrete core cooling system under hot–semiarid climatic conditions

D. G. Leo Samuel[1], S. M. Shiva Nagendra[2] and M. P. Maiya[1]

Abstract

Concrete core cooling system is an energy efficient alternative to the conventional mechanical cooling system. It provides better comfort due to direct absorption of radiation load, low indoor air velocity, apt vertical temperature gradient and absence of noise. It can be operated at relatively higher water temperature, which facilitates the use of passive cooling strategies. In this study, a cooling tower, which is an 'evaporative cooling system', is preferred over other passive cooling options due to its better cooling performance in dry regions and its ability to operate all through the day. This paper presents the results of computational fluid dynamic analysis of a room cooled by concrete core cooling system supported by a cooling tower. The study reveals that for a typical hot–semiarid summer climatic condition in India, the system reduces the average indoor air temperature to a comfortable range of 23.5 to 28°C from an uncomfortable range of 35.3 to 41°C in a building without cooling. The average predicted percentage of dissatisfied falls from 99.7% in a building without cooling, to 37.3% if roof and floor of a building are cooled with concrete core cooling system and further to 6.3% if all surfaces are cooled with concrete core cooling system.

Keywords

Passive cooling, Concrete core cooling, Cooling tower, Evaporative cooling, Thermal comfort, Thermally activated building system

Accepted: 3 February 2016

Introduction

The global construction market is growing rapidly and is expected to reach US$15 trillion by 2025. In particular, India is projected to have an annual growth of 7.4% in the construction industry and is expected to become the third largest in the global construction market.[1] The major driving factor for this growth is urbanization. The urban population in India has grown from 293 million in 2001 to 377 million in 2011 according to the official census of India.[2] This rapid urbanization has led to an increase in housing and the related energy demand. About 30 to 45% of the global energy is consumed by buildings.[3] In India, 34% of energy is consumed by the residential and commercial sectors.[4] A major part of the energy consumed by buildings is for heating, ventilation and air-conditioning (HVAC). About 15% of the global energy consumption is towards refrigeration and air-conditioning needs.[5] Depending on the economic status

[1]Department of Mechanical Engineering, Indian Institute of Technology Madras, Chennai, India
[2]Department of Civil Engineering, Indian Institute of Technology Madras, Chennai, India

Corresponding author:
D. G. Leo Samuel, Indian Institute of Technology Madras, Refrigeration and Air Conditioning Laboratory, Chennai 600036, India.
Email: dglsam@gmail.com

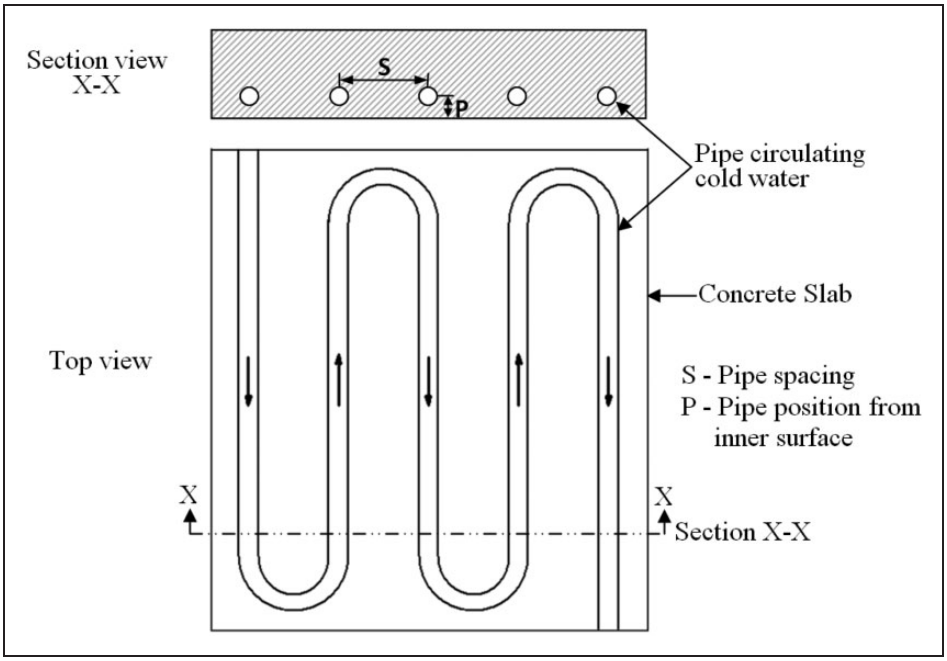

Figure 1. Schematic diagram of CCC system.

and climatic conditions, the percentage of energy consumed by the HVAC sector could vary. In the UK, USA and Spain, air-conditioning accounts for 62%, 53% and 42% of the respective country's residential sector energy consumption.[6] India is expected to have higher growth in cooling energy demand due to economic growth and the tropical climatic conditions experienced in a major part of the country. The forecast is that, by 2055, the country's cooling energy demand will be higher than the USA and China.[7]

Air-conditioning industry has experienced a rapid growth in the past few decades due to heat island effect in cities, global warming, increase in time spent indoors, aspiration for better living conditions and increased glazing in modern architecture. In Greece, climatic change is forecasted to increase the energy demand for cooling applications by 83% in 30 years (2010–2040).[8] For the past few decades, the air-conditioning requirement is predominantly met by vapour compression systems. However, the conventional mechanical systems are energy intensive and eco-destructive. They are also reported to provide poor indoor air quality (IAQ) and poor comfort due to noise and draft. Poor IAQ is attributed to a higher CO_2 level in the conditioned space resulting from recirculation of air to reduce the energy consumption.[9,10] An experimental study reported that in naturally/mechanically ventilated bedrooms the average CO_2 concentration is in the range of 420 to 560 ppm, this increases to 500 to 1100 ppm range in air-conditioned buildings.[9] The higher CO_2 level could reduce the sleep hour of the occupants. These limitations of the conventional system have led to the search for alternative cooling techniques, which can provide better thermal comfort with lower energy consumption.

Concrete core cooling (CCC) system, also known as thermally activated building system, is one such alternative that can provide better thermal comfort with reduced energy consumption.[11,12] The CCC system consists of pipes embedded in a concrete slab (Figure 1). Cold water passing through the pipes removes the heat from the slab, which in turn removes the heat from the room. The CCC system offers better thermal comfort in comparison to the conventional cooling system because of the absence of draft, low vertical temperature gradient and direct dissipation of radiation load.[13] It also provides better energy performance due to change in heat transfer medium from air to water, high coefficient of performance of chiller, low quantity of air handling and relatively higher indoor air temperatures (1 to 2°C) for the same thermal comfort conditions, resulting from enhancement of radiation heat removal. The thermal mass of a CCC system transfers part of the cooling load to night and also reduces the peak energy demand by 60 to 70% as the cooling load is distributed over a longer period.[14] The CCC system could be used with a passive cooling system like earth tunnel, nocturnal radiator and cooling tower (CT) as the CCC system can operate at relatively higher temperature.[15,16] A numerical study for the climate of Zurich, Switzerland, concluded that thermal comfort can be achieved with CCC system supported

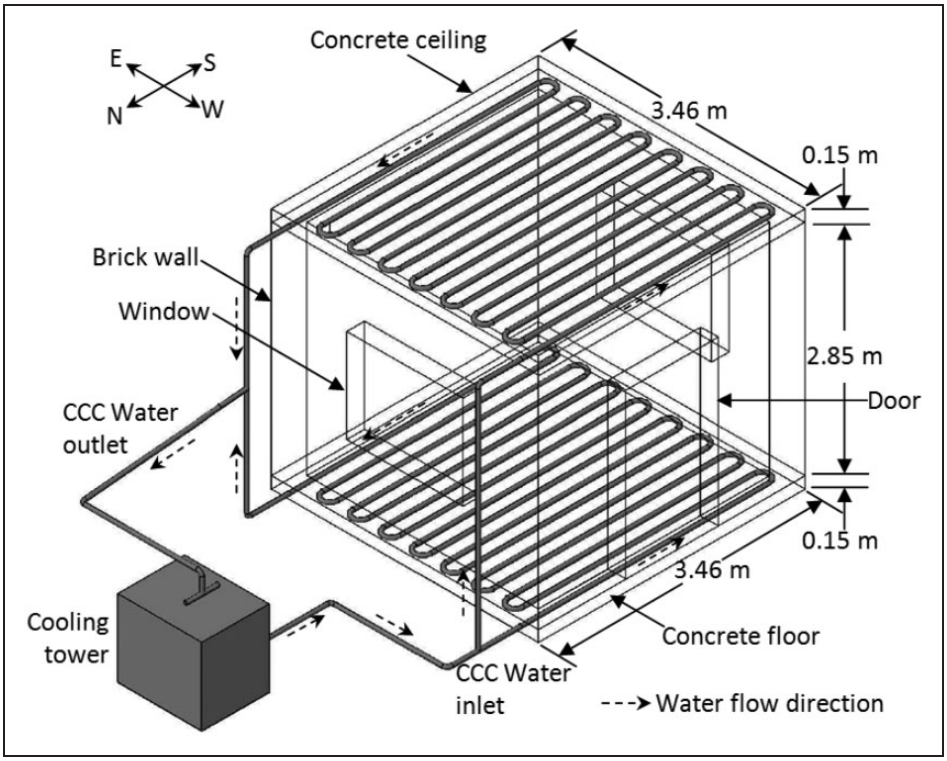

Figure 2. Schematic for CCC system supported with cooling tower.

with CT operating at night.[15] Another numerical study concluded that in hot–humid climatic conditions, a radiant cooling system supported with a CT can achieve operative temperature of 28°C,[16] which is the neutral temperature for people who have adapted to living in hot–humid climatic conditions.[17]

The performance of passive cooling systems greatly depends on the local climatic conditions such as temperature and relative humidity of ambient air. In arid and semiarid regions (low relative humidity), evaporative cooling is preferred over other passive cooling systems due to better cooling performance, low capital cost and continuous operation all through the day. However, increase in absolute humidity is a major concern due to health issues and corrosion of materials associated with higher relative humidity. This could be mitigated with indirect evaporative cooling systems.

The present work aims at computing the comfort level attained with an indirect evaporative cooling system, which couples CCC system with CT. The influence of ventilation and internal load on indoor comfort level in a building was analysed for the hot–semiarid climatic conditions (New Delhi). The increase of cooling ability by including wall cooling was also studied. Comfort indices such as predicted mean vote (PMV) and predicted percentage of dissatisfied (PPD) were calculated, which aid in understanding the thermal comfort achieved inside the room.

Computational fluid dynamic modelling

CFD technique and zonal or multizonal energy simulation models (TRNSYS and EnergyPlus) are widely used in simulation of comfort level inside the buildings. The latter, zonal or multizonal energy simulation models, assumes each zone as completely mixed. As a result, these models will not provide variation of air flow and temperature distribution within the zone. On the other hand, CFD overcomes these limitations by providing finer distribution of air flow and temperatures variations within the domain.

CFD is the science of solving complex fluid flow problems using numerical methods. COMSOL Multiphysics, a CFD tool, was used to simulate the temperature and velocity distribution of the model geometry represented in Figure 2. The water from CT was supplied through pipes embedded in the concrete slabs of roof and floor. The water removes heat from these slabs and returns back to the CT where the heat is released to ambient air. The slabs in turn cool the indoor space by convection and radiation.

The CFD solution procedure was classified into three steps namely pre-processing, simulation and post-processing. All the inputs needed for simulation were set in the pre-processing stage, that includes building model geometry, specifying material properties, defining

problem physics, setting-up of initial and boundary conditions, meshing the model geometry and specifying convergence criteria and numerical solution techniques to be employed. The governing equations were solved using the specified numerical techniques in the simulation stage. Analyses and reporting of results were done in the post-processing stage.

Governing equations

The continuity, momentum and energy equations applicable to the model are represented by equations (1) to (4) as follows

$$\frac{\partial \rho}{\partial t} + \nabla.(\rho u) = 0 \tag{1}$$

$$\rho\left[\frac{\partial u}{\partial t} + (u.\nabla)u\right] = -\nabla \mathrm{p} + \mu\nabla^2 \mathrm{u} + \frac{\mu}{3}\nabla(\nabla.\mathrm{u}) + \mathrm{f} \tag{2}$$

$$\rho C_p\left(\frac{\partial T}{\partial t} + u.\nabla T\right) = \nabla.(k\nabla T) + Q \tag{3}$$

$$\rho C_p \frac{\partial T}{\partial t} = \nabla.(k\nabla T) + Q \tag{4}$$

where ρ is the density in kg/m^3, t is the time in seconds, u is the velocity vector in m/s, p is the pressure in Pa, μ is the dynamic viscosity in Ns/m^2, f is the body force vector in N/m^3, C_p is the specific heat in J/kgK, T is the temperature in K, k is the thermal conductivity in W/mK and Q is the heat source in W/m^3.

The velocity, temperature and pressure distribution of the indoor air were obtained by simultaneously solving equations (1) to (3). The temperature distribution in the walls, roof and floor was calculated by equation (4). The body force term, f, in equation (2) accounts for buoyancy force and the heat source term, Q in equations (3) and (4) represents the internal sensible loads.

The temperature difference between the inner surfaces is considerably high. Hence, it is essential to account radiation heat transfer. For a diffuse gray surface, the total radiation leaving the surface (radiosity) is calculated by equation (5)

$$J = (1-\varepsilon)G + \varepsilon\sigma T^4 \tag{5}$$

where J is the radiosity (outgoing radiation) in W/m^2, ε is the emissivity, G is the irradiation (incoming radiation) in W/m^2, σ is the Stefan Boltzmann constant in W/m^{2}K^4 and T is the temperature of emitting surface in K.

The radiation heat transfer is defined by equation (6) and is coupled with convection through source term given in heat equation (equation (3)).

$$Q = \varepsilon\left(G - \sigma T^4\right) \tag{6}$$

The length to diameter ratio of pipe is very high. Therefore, the fluid flow inside the pipe can be assumed to be fully developed. This helps to simplify the governing equation to 1D along the centre-line of pipe. The simplified continuity, momentum and energy equations are given by equations (7) to (9).[18,19]

$$\frac{\partial A\rho}{\partial t} + \nabla.(A\rho\bar{u}) = 0 \tag{7}$$

$$\rho\frac{\partial u}{\partial t} = -\nabla p - f_D\frac{\rho}{2d_h}\bar{u}|\bar{u}| + f \tag{8}$$

$$\rho A C_p\frac{\partial T}{\partial t} + \rho A C_p\bar{u}.\nabla T = \nabla.Ak\nabla T + f_D\frac{\rho A}{2d_h}|\bar{u}|^3 + Q + Q_{\mathrm{wall}} \tag{9}$$

where A is the cross-sectional area of pipe in m^2, $\bar{u}$ is the cross section averaged fluid velocity along the tangent of the centre line of a pipe in m/s, f_D is the Darcy friction factor, d_h is the hydraulic diameter in m and Q_{wall} is the heat transfer through pipe wall in W/m.

The heat transfer through the pipe wall (Q_{wall}) appearing in equation (9) accounts the thermal conductivity of pipe material and is given by equations (10) to (12)

$$Q_{wall} = h_{eff}Z(T_{ext} - T_f) \tag{10}$$

$$\frac{1}{h_{eff}} = \left[\frac{1}{h_i} + \frac{r_i ln\left(\frac{r_o}{r_0 - 1}\right)}{k_{wall}}\right] \tag{11}$$

$$h_i = Nu \times k_{water}/(2 \times r_i) \tag{12}$$

where h_{eff} is the effective heat transfer coefficient of pipe in W/m^{2}K, Z is the wetted perimeter in m, T_{ext} is the temperature of the domain surrounding the pipe in K, T_f is the temperature of cooling water inside the pipe in K, h_i is the inner surface heat transfer coefficient of pipe in W/m^{2}K, r_i and r_o are the inner and outer radius of the pipe in m, k_{wall} is the thermal conductivity of pipe material in W/mK, Nu is the Nusselt number, k_{water} is the thermal conductivity of water inside the cooling pipe in W/mK.

The Nusselt number (Nu) for laminar flow is 3.66, and for turbulent flow it is given by equation (13)[20]

$$Nu = \frac{(f_D/8)(Re - 1000)Pr}{1 + 12.7\sqrt{(f_D/8)}(Pr^{0.667} - 1)} \tag{13}$$

where Pr is the Prandtl number.

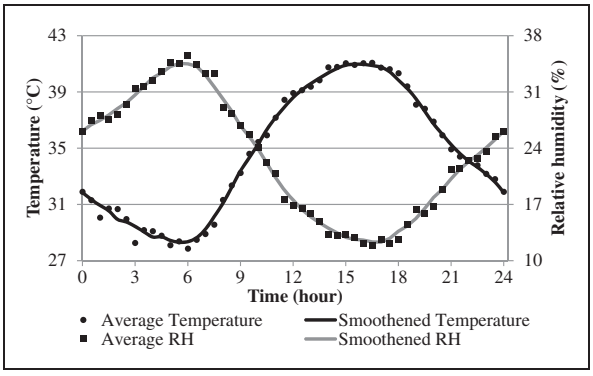

Figure 3. Monthly average data of May smoothened to reduce computation time.[22]

The Darcy friction factor (f_D) in equation (13) can be computed using Churchill friction model.[21] The temperature of domain surrounding the pipe, T_{ext}, is the temperature of slab in which it is embedded.

Boundary and initial conditions

The walls and roof of a 3.46 m × 3.46 m × 3.15 m room (actual dimensions of a building being constructed for testing) are exposed to solar radiation and outdoor temperature. The metrological data of New Delhi for the year 2013 were obtained from an online metrological database.[22] A representative diurnal trend of temperature and relative humidity for each month was obtained by averaging the data of different days for the same time. This was then smoothened with a moving average (Figure 3).

The ambient temperature data were combined with solar radiation to obtain sol-air temperature. The solar radiation on the roof and walls in W/m^2 was calculated by equation (14)

$$I = 1082 \times \exp(-0.182/\sin\beta) \times [(\cos\beta \times \cos\alpha \times \cos\varphi + \sin\beta \times \sin\varphi) + c \times F_{ws}] \quad (14)$$

where I is the total solar radiation intensity on surface in W/m^2, α is the angle between solar azimuth angle and normal to the surface in degree, β is the altitude angle in degree, φ is the angle between normal of the surface and horizontal plane in degree, c is the diffusion coefficient for solar radiation and F_{ws} is the wall to sky view factor.

The total solar radiation was obtained by multiplying normal solar intensity with direct and diffused solar radiation components. The solar angles in equation (14) were calculated by equations available in litratures.[23] The sol-air temperature specifies the boundary condition for the external surfaces of roof and walls. Figure 4 presents the diurnal variation of sol-air temperature on different external surfaces and ambient temperature. The difference between minimum sol-air temperature and ambient temperature during daytime was due to diffused solar radiation. The cooling by nocturnal long-wave radiation to the sky was not considered as this was found to have minimal impact on the temperature of indoor air and room's inner surfaces. Ignoring nocturnal radiation, for the simulation of a room with an internal load of 400 W and ventilation of 0.03 m^3/s, would reduce the diurnal average operative temperature and PMV by just 0.1°C and 0.04, when the roof and floor of the room was cooled by CCC system. The maximum difference in operative temperature was only 0.2°C. The minimal change in indoor comfort parameters is because the nocturnal radiation cooling would reduce the temperature of external roof surface, which would change the convective heat transfer from this surface and thus compensates the cooling by nocturnal radiation.

Two openings were considered for ventilation. An opening of 0.1 m × 3.0 m was located on the southern wall near the floor, which was considered to provide fresh air at outdoor temperature and with a velocity of 0.1 m/s. Hence, the inlet opening would have a velocity boundary condition with uniform normal velocity of 0.1 m/s. An opening of 0.8 m × 0.8 m that was located at the centre of the northern wall was considered to be the air outlet. The outlet opening would have a pressure boundary condition with gauge pressure of 0 Pa.

It is possible to obtain temperatures lower than wet-bulb temperature (WBT) with dew point CT, in which the CT inlet air can be pre-cooled with CT exit air.[24] Hence in this study, CT outlet water was assumed to be at WBT. The WBT in degree celsius was calculated by equation (15)[25]

$$t_w = (t_a)\tan^{-1}\left[0.151977(RH + 8.313659)^{0.5}\right] + \tan^{-1}(t_a + RH) - \tan^{-1}(RH - 1.676331) + 0.00391838(RH)^{0.75} \times \tan^{-1}(0.023101RH) - 4.686035 \quad (15)$$

where t_w is the wet-bulb temperature in °C, t_a is the ambient temperature in °C and RH is the relative humidity in %.

It is not possible to know the initial conditions, i.e. temperature and velocity distribution of the model domain. This problem can be resolved by the iteration method. The simulation was run over the study duration of one day with a guess initial value, which was

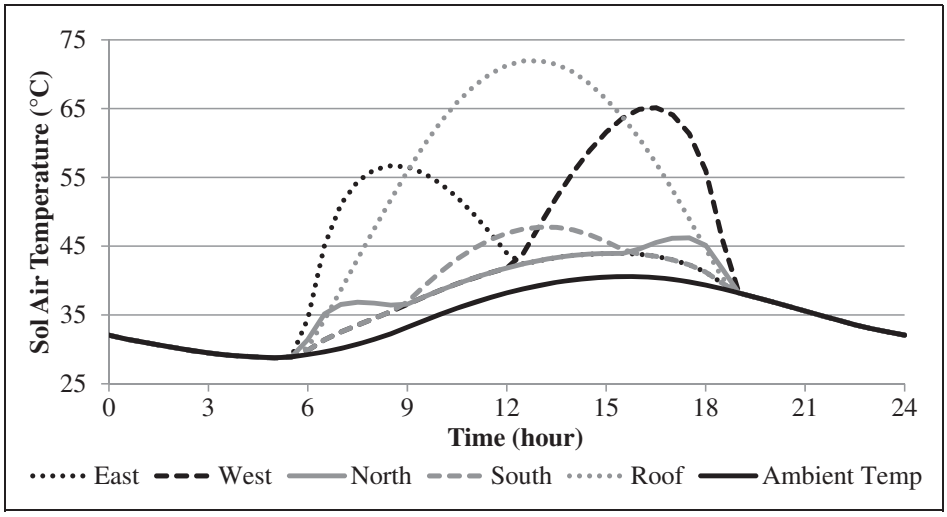

Figure 4. Diurnal variation of sol air temperature and temperature of ambient air.

repeated with the updated value till the difference between successive iterated values becomes negligible.

Meshing

Unstructured tetrahedral mesh, with mesh size based on physics was used. The mesh used should be finer at locations where the fluid domain interacts with the solid domain, i.e. near the walls, floor and roof, and near the surfaces of air inlet and outlet and would be relatively coarser at other locations such as the centre of the room. The same rule was adapted. Figure 5 presents the mesh on a cross-section plane facing west which was located at the centre of the room. Mesh independence analysis was carried out to ascertain the required fineness of the mesh. For the model considered, the minimum mesh elements without losing accuracy were found to be 332,224.

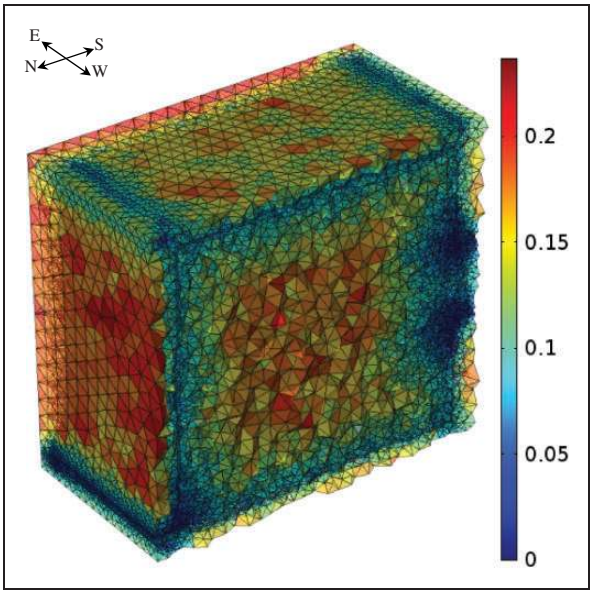

Figure 5. Mesh size on cross-section plane facing west direction which was located at the centre of the room.

Solver settings

Second-order backward difference method (multistep method) was used in the preset simulation. The simulation was carried out by varying the step size based on convergence. In other words, if the convergence was poor, then the simulation would be proceeded slowly in time by taking step of smaller size; otherwise, it would be proceeded faster with larger step size. A very large step size can lead to inaccurate results. The simulation with maximum step size of 1800 s was observed to give similar result as compared to simulation with smaller values of maximum step size. Further, increasing the limit beyond 1800 s would provide incorrect results. Absolute tolerance of 10^{-3} was set for all the dependent parameters. The air movement in the indoor space was assumed to be laminar as the air velocity in the indoor space was low. Moreover, the turbulence in indoor air would require an increase in the computation time without any appreciable change in output.

Comfort parameters

Thermal comfort has an appreciable bearing on health, psychology and productivity of occupants. Thermal comfort is said to be achieved when the body rejects heat at the same rate at which it is produced without any strain on human thermal regulatory system.

Human comfort mainly depends on six thermal comfort parameters, namely air temperature, mean radiant temperature (MRT), air velocity, humidity, clothing insulation and metabolism rate. These parameters may be combined to obtain comfort indices for assessing the thermal comfort.[26] Other parameters such as radiant asymmetry could also impact thermal comfort; however, most of the standards have ignored this parameter due to the associated complexity.[27]

PMV is the most recognized thermal comfort index, which takes into consideration of all six primary thermal comfort parameters. The index was developed using experimental data obtained from a controlled environment and the heat flow imbalance between actual and the optimum comfort conditions.[28] Standard 7-point scale (−3 to + 3) has been used to calculate PMV with zero representing thermal neutrality. PPD is related to PMV and indicates the dissatisfaction level among the occupants.[29] PMV and PPD are given by equations (16) and (17), respectively

$$PMV = [0.303 \times \exp(-0.036M) + 0.028] \times [M - W - E_d - E_s - L_R - D_R - R - C] \quad (16)$$

$$PPD = 100 - 95 \times \exp\left[-\left(0.03353PMV^4 + 0.2179PMV^2\right)\right] \quad (17)$$

where PMV is the predicted mean vote, M is the metabolic rate in W/m^2, W is the external work in W/m^2, E_d is the heat loss by water vapour diffusion through skin in W/m^2, E_s is the heat loss by sweating in W/m^2, L_R is the latent respiration heat loss in W/m^2, D_R is the dry respiration heat loss in W/m^2, R is the heat loss by radiation in W/m^2, C is the heat loss by convection in W/m^2 and PPD is the predicted percentage of dissatisfied in %.

The metabolic rate and external work were assumed to be 1.1 met (63.8 W/m^2) and 0 W, respectively. The other terms in equation (16) represent heat loss from the body.[26] Clothing was assumed to be 0.6 clo, and iteration method was used to calculate the clothing temperature. The indoor relative humidity was calculated assuming constant absolute humidity at average outdoor conditions. In equation (17), PMV was assigned zero whenever it is less than zero, which happens due to over cooling as such situations could be avoided by using a suitable control system.

The operative temperature was calculated from indoor air temperature, MRT, and convective and radiative heat transfer coefficients (equation (18)). The MRT was calculated from inner surface temperatures and view factors. The latter was calculated[26] by assuming a person standing at the centre of the room. The indoor air velocity was very low for the case considered in this study. Therefore, the convective heat transfer coefficient was taken as 4 W/m^{2}K. The radiative heat transfer coefficient of 4.7 W/m^{2}K was taken considering typical indoor temperatures.

$$T_o = (h_r T_{mrt} + h_c T_a)/(h_r + h_c) \quad (18)$$

where T_o is the operative temperature in K, h_c is the convective heat transfer coefficient in W/m^{2}K, h_r is the radiation heat transfer coefficient in W/m^{2}K, T_a is the ambient temperature in K and T_{mrt} is the mean radiant temperature in K.

The average of various parameters such as temperature and velocity was obtained by integrating the parameter over the surface or volume and then dividing the result obtained by total surface area or volume, respectively.

Case study

Description of experimental facility

A test room of dimensions 3.46 m × 3.46 m × 3.15 m was built at Indian Institute of Technology Madras (IITM), Chennai, India, to study the performance of CCC system. The room was made of single brick wall with a thickness of 0.28 m with two openings of dimensions: 1.5 m × 1.21 m, for glazed windows and one opening of dimensions: 1.2 m × 2.12 m, for 34% glazed door. The building was situated inside the Institute campus, a reserved forest area full of trees. While the eastern wall was almost completely shaded, the western wall was partly shaded during evening time by trees and the northern wall was shaded by the equipment of the cooling system. Further, the experiments were conducted during a cloudy day. Therefore, the impact of solar radiation on walls was relatively small.

The concrete roof and floor were 0.15 m thick. The cross-linked polyethylene pipes have an outer diameter of 0.024 m and thickness of 0.0035 m; these were embedded in the roof and floor. The pipes were placed in serpentine arrangement with pipe spacing of 0.2 m and at a distance of 0.05 and 0.06 m from the inner surfaces of roof and floor, respectively. The internal load in the room was about 400 W (sensible), which includes a desktop, cathode ray tube monitor, rectifier to power monitoring equipment, IAQ meter and dust monitor. No latent load source was available inside the test room.

Description of the monitoring system

The indoor air temperatures were measured along four vertical lines that were parallel to the inner surface of

walls and are at a distance of 1 m from adjacent walls. On each of these vertical lines, temperatures were measured at three different heights (0.5, 1.5 and 2.5 m from the floor). The temperatures of roof and floor were measured at points where the vertical lines intersect the inner and outer surfaces. The temperature of walls' inner and outer surfaces was measured at two points on each surface at a height of 1.5 m from the floor. The temperature of water was measured near the inlet and exit of each building fabrics and in the tank where the water was stored after passing through the CT. The outdoor air temperature was also measured.

Results

Figure 6 presents the diurnal temperature variation of indoor air, inner and outer surfaces of building fabrics which was cooled by CCC system with CT on 15 May, 2014. The fluctuation of temperature on the roof outer surface was very high at 19.1°C (Figure 6(a)) as it was exposed to variation of solar radiation intensity and ambient temperature. The thermal mass of roof would reduce the diurnal fluctuation of roof inner surface to 9°C. The minimum and maximum temperature of the roof's inner surface was delayed by 1 h 13 min and 2 h 54 min, respectively, against the respective extrema of the roof's outer surface. The average and diurnal fluctuation of indoor air temperature were 32.5 and 4.5°C respectively. The temperature of the floor was relatively constant all through the day, as the influence of diurnal variation of solar radiation and ambient temperature on it was minimal. The vertical temperature difference between 0.5 and 1.5 m was shown to vary from 0.2 to 0.8°C (Figure 6(b)). The temperature of the inner roof surface peaked at about 14:00. The convective heat transfer took place between this surface and the vicinity air and hence the vertical temperature difference in the room also peaked around the same time. The temperatures of external surfaces of different walls were shown to vary as different intensity of solar radiation were received by these walls (Figure 6(c)). In the morning hours, the temperature of outer surface of eastern wall

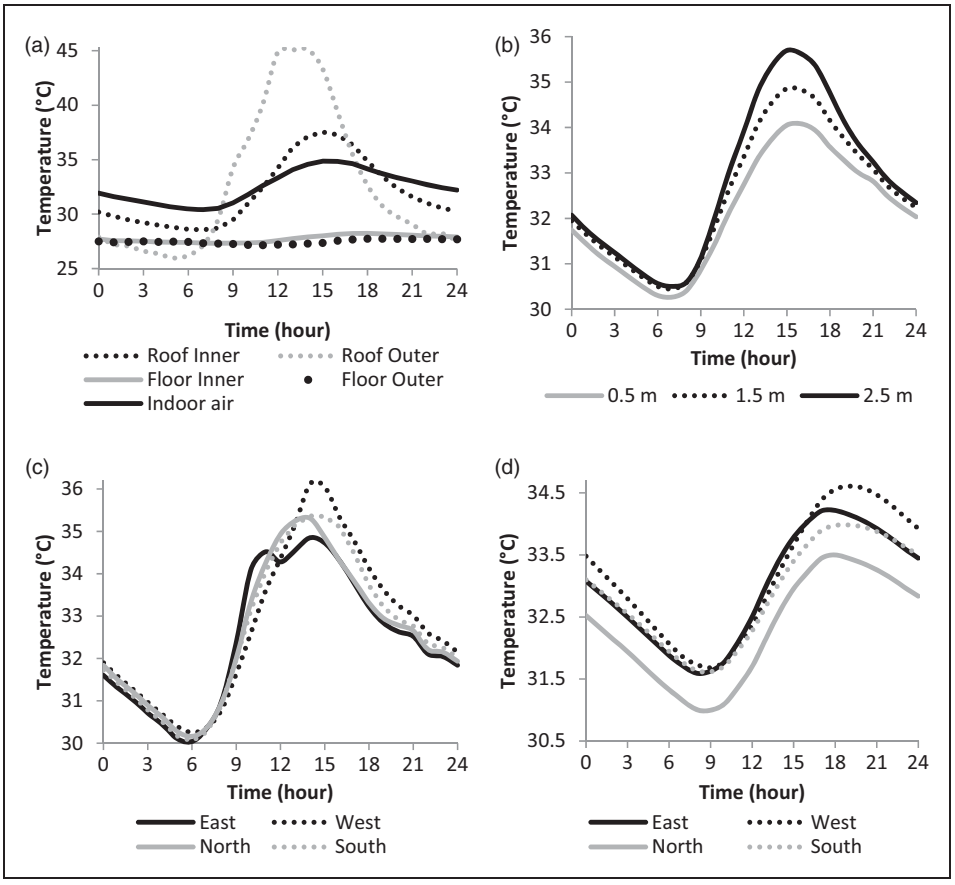

Figure 6. Diurnal temperature variation of (a) indoor air, and the roof's and floor's inner and outer surfaces (b) indoor air at various heights (c) outer surface of walls (d) inner surface of walls.

was marginally higher as more solar radiation was received in spite of shading by adjacent trees. Temperature of the outer surface of the western wall was shown to reach a peak at about 15:00 as more solar radiation was received in the afternoon. The temperature of the southern wall was higher than northern and eastern wall during the afternoon. This was because solar radiation was received by the southern wall during the afternoon due to slight tilt in building orientation. The temperature of wall outer surfaces could impact its inner counterpart which is clearly visible by comparing Figure 6(c) and (d).

Model validation

The CFD model was validated with five days' experimental data. Hourly average temperature of external surfaces and water inlet temperature of CCC system measured at the experimental facility were used to specify the boundary conditions. Figure 7 compares the indoor operative temperature calculated from the model output against the one calculated from experimental data. The output of the model was found to match well with experimental data.

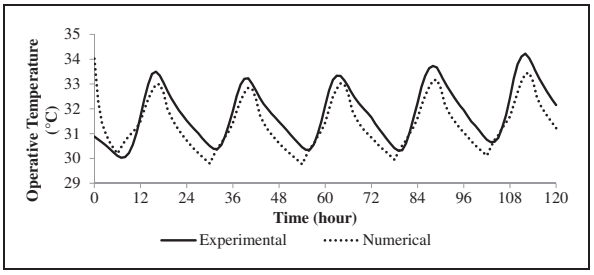

Figure 7. Model validation.

Table 1. Model input parameters.

Sl. no.	Parameter	Value
1	Room size (L × B × H), m × m × m	3.46 × 3.46 × 3.15
2	Roof and floor thickness, m	0.15
3	Wall thickness, m	0.23
4	Pipe internal diameter, m	0.017
5	Pipe wall thickness, m	0.0035
6	Spacing between pipes, m	0.2
7	Pipe arrangement	Serpentine
8	Pipe position from inner surface, m	0.06
9	Water inlet velocity, m/s	0.8
10	External surfaces heat transfer coeff, W/m^2K	30

Discussion

The model input parameters and material properties were shown to have appreciable impact on the performance of the system, and these are listed in Tables 1 and 2, respectively. Three scenarios, namely, no cooling, roof and floor cooling and all surfaces cooling were simulated. In each scenario, four cases as listed in Table 3 were studied. Internal load of 400 W was present in the experimental study, and the same was considered for simulation. The load was distributed uniformly throughout the room volume. The combined heat transfer coefficient for all the external surfaces was considered to be 30 W/m^2K, of which 3/4 was due to convection and the remaining was due to radiation. The convective heat transfer coefficient was calculated considering the average outdoor air velocity of 3.4 m/s.[30] The results presented were for the month of May, when the climate was hot and dry. The ventilation requirement and the design of door and windows of the different regions was shown to vary widely from warm and humid climate region (where the experiments were conducted) to hot and semiarid climate region (for which the numerical study was carried out). Therefore, the door and windows used in the validation model should not be used for further study. In hot and semiarid climatic condition, the doors and windows are generally made of opaque

Table 2. Material properties.

Sl. no.	Property	Walls	Roof and floor
1	Material	Brick	Concrete
2	Density, kg/m^3	2000	2300
3	Specific Heat, J/kgK	1000	1130
4	Thermal Conductivity, W/mK	1	1.8

Table 3. Scenario analysis.

Sl. no.	Case	Attributes
1	A	No internal load and no ventilation
2	B	Internal load of 400 W and no ventilation
3	C	No internal load and ventilation of 0.03 m^3/s
4	D	Internal load of 400 W and ventilation of 0.03 m^3/s

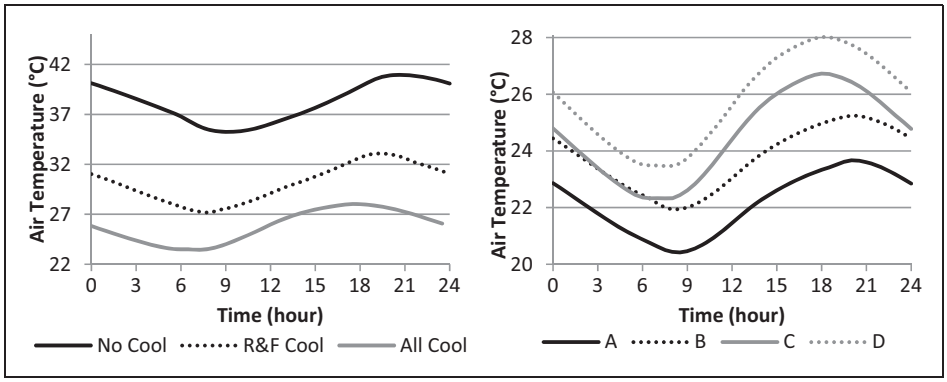

Figure 8. The average indoor air temperature in Case D (left) and all surfaces cooling (right).

material (mainly wood), small in size and well shaded in order to reduce solar heat gain. Therefore, the impacts of doors and windows on indoor conditions would be small. Thus, they can be neglected to reduce computation time. Energy balance analysis was carried out, and no significant deviation was observed.

Air temperature

Air temperature is an important thermal comfort parameter, as it controls the convective heat transfer of the human body.

Figure 8 presents the diurnal pattern of indoor air temperature for the cases studied in the month of May. The average indoor temperature for Case D with no cooling was 38.1°C. This was declined to 30.1°C due to the cooling in the roof and floor and was declined further to 25.8°C due to cooling of all surfaces.

The diurnal variation of indoor air temperature for the cases studied followed a similar trend and resembled the diurnal outdoor temperature variation, but with a time lag. The outdoor temperature declined in the morning to reach the minimum at 5:00. This had led to a decline of indoor temperature during the morning hours. However, the decline in indoor temperature continued further due to thermal storage capability of the structural components. The minimum indoor air temperature was reached between 7:30 and 10:30 depending on the presence or absence of cooling system and ventilation. After this, the indoor temperature rose to reach a maximum between 18:00 and 22:00. The temperature rise was associated with a rise in outdoor temperature, solar radiation and temperature diffusivity of the building structure.

In the no cooling scenario, the solar radiation would heat the building, but the ventilation air would cool the indoor space during morning hours as the indoor air was at higher temperature as compared to the ventilated air. The net heat transfer had led to a cooling of indoor air till 9:00 (for Case D). However, for all surfaces cooling, the ventilated air would heat the indoor space during morning hours as it was at a higher temperature than indoor air. In addition, the solar radiation and outdoor air would also heat the building. Therefore, a rise in indoor air temperature from 7:30 (for Case D) was observed. Thus, the cooling system was shown to advance the attainment of minimum temperature. The advancement was also shown in the cases without ventilation. This could be attributed to higher external heat transfer into the building due to higher difference between sol-air and building outer surfaces temperatures.

The cooling system was also observed to advance the attainment of maximum temperature. For example, in Case D, the maximum temperature was attained at 20:30 in the no cooling scenario, which was advanced to 19:30 in the cooling of roof and floor and to 18:00 in the cooling of all surfaces. This was because the cooling water would remove the heat accumulated in the concrete slab during daytime and prevented the rise of indoor air temperature during late evening hours.

The temperature fluctuation of indoor air was low as compared to that of outdoor air. In the present study, the former was in the range of 3.1 to 6°C, while the latter was 11.8°C. This could be attributed to thermal storage of building components. The increase in the cooling surface could reduce the temperature fluctuation, as it would increase the resistance for outdoor heat penetration. For Case D, the average temperature fluctuation of indoor air was 5.9°C in the cooling of roof and floor, which was reduced to 4.6°C in the cooling of all surfaces. In the presence of internal load, the ventilation system would reduce the indoor air temperature by 2.2°C when there was no cooling and the indoor air temperature would be increased by 0.7°C in the cooling of the roof and floor scenarios and by 2.1°C in the cooling of all surfaces scenarios. Therefore, ventilation is advisable in the no cooling scenario, and during the cooling scenarios this must be equal to the minimum required to meet the IAQ standards.

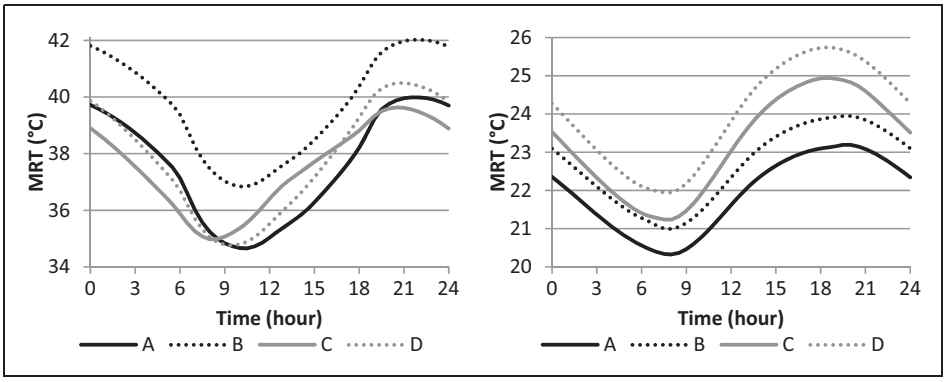

Figure 9. Diurnal MRT variation in the no cooling scenario (left) and in the cooling of all surfaces (right).

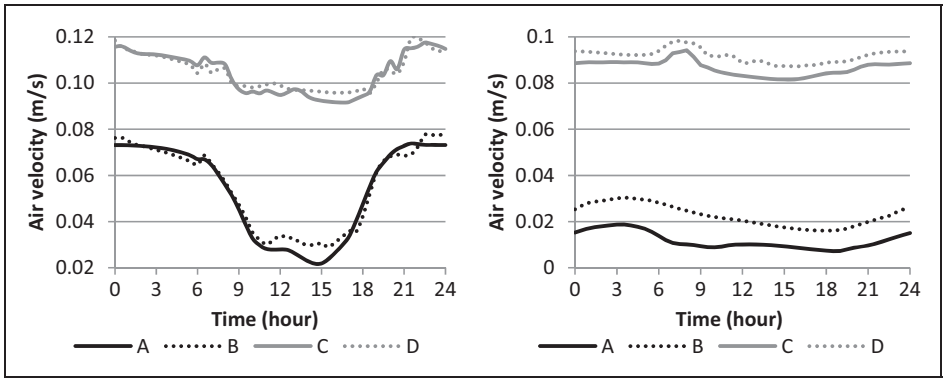

Figure 10. The average air velocity in the cooling of the roof and floor (left) and cooling of all surfaces (right) scenarios.

The ventilation system could also reduce the time lag between the extremum of indoor and outdoor air temperatures due to the fact that the ventilation would increase the indoor–outdoor interaction. For example, in the cooling scenario of all surfaces, the minimum and maximum temperatures were attained at 8:00 and 20:00 in Case B, which was advanced to 7:30 and 18:00 in Case D. In the cooling scenario of all surfaces, the ventilation would increase the average indoor temperature fluctuation from 3.3°C (Case B) to 4.6°C (Case D) due to the higher temperature rise caused by the hot ventilated air during the daytime.

The internal load in the absence of ventilation would increase the average indoor temperature by 2.9, 1.7 and 1.6°C in scenario of no cooling, cooling of roof and floor and cooling of all surfaces, respectively. The lower temperature increase in the cooling scenarios was due to the removal of a part of the internal load by the cooling system. As internal load was assumed to be invariable with time, it has no impact on the time lag.

MRT

The MRT could impact the radiative heat transfer from the human body. The CCC system was observed to have a higher influence on the decline of MRT and its time lag than on the indoor air temperature, as the cooling system would first cool the inner surfaces of the room and then the indoor air. The average MRT in Case D with no cooling was 37.8°C. This was declined to 28.4°C in the scenario of cooling of roof and floor and further to 24°C in the cooling of all surfaces (Figure 9). The minimum MRT in Case D with no cooling was attained at 9:30. An earlier attainment at 8:30 in the cooling of roof and floor and 7:30 in the cooling of all surfaces were observed (Figure 9).

The ventilation system in the presence of internal load could reduce the average MRT by 1.8°C in the scenario of no cooling, but would increase the average MRT by 0.6°C in the cooling scenario of the roof and floor and by 1.4°C in the cooling of all surfaces. The decline in MRT in the scenario with no cooling was due to the removal of a part of the internal load and solar heat gain by ambient air, which was at a lower temperature as compared to indoor air. In the cooling scenarios, the indoor air temperature was lower than ambient air. Hence, ventilation would increase the MRT. On an average, the ventilation would advance the extrema of MRT by approximately 1 h.

In the absence of ventilation, the internal load would increase the average MRT by 2.2°C in the no cooling

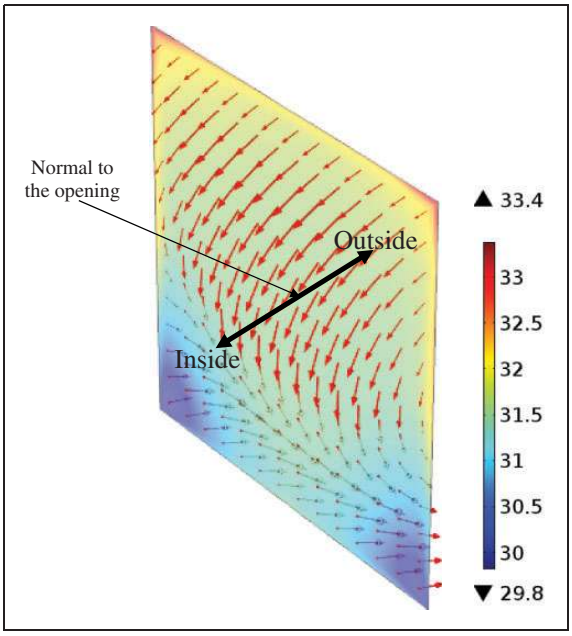

Figure 11. Temperature distribution (°C) and velocity arrows at the outlet opening.

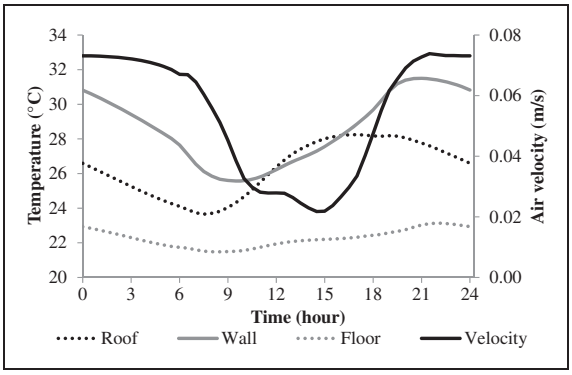

Figure 12. The average inner surfaces temperature and average indoor air velocity in the cooling of the roof and floor with no ventilation and no internal load.

scenario, 1°C in the cooling of the roof and floor and 0.7°C in the cooling of all surfaces. The lower increase in MRT in the cooling scenarios was due to the availability of heat sink with the same internal load. Further, the internal load was observed to have no influence on MRT time lag. The impact of ventilation and internal load on MRT was relatively less when compared to their impact on indoor air temperature.

Indoor air velocity

Air velocity could impact the heat loss from the body by altering the convective heat transfer coefficient. High velocities could result in draft. The preferred air velocity would vary with air temperature, turbulence intensity, etc. In an environment with neutral temperature, air velocity should be less than or equal to 0.25 m/s for acceptable thermal comfort. The average air velocity for all the cases studied was less than 0.13 m/s. Figure 10 presents the air velocity of the cases studied. Ventilation was found to enhance the air velocity in the indoor space. The internal load would have a minimum impact on indoor air movement as it was assumed to be distributed uniformly throughout the volume. Among the two cooling scenarios, the cooling of the roof and floor recorded higher indoor air movement as cool ceiling and warm walls would enhance air movement by natural convection.

Figure 11 presents the temperature and air flow distribution at the outlet opening in the cooling of all surfaces scenario of Case D. The outdoor air would enter through the inlet as well as upper region of the outlet opening and would exit through the bottom region of the opening. As a result, the air velocity was found to be very high at the bottom region of the outlet opening. The minimum and maximum normal velocity components at the outlet opening were found to be −1.6 and 2.5 m/s, respectively. The negative sign would indicate air was entering through the opening.

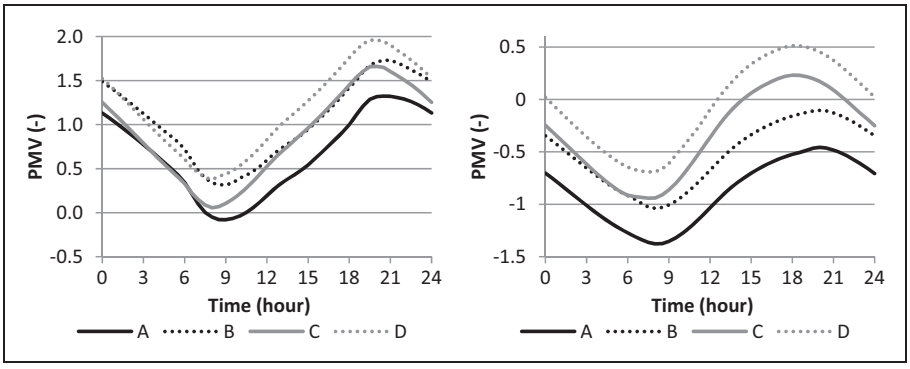

Figure 13. PMV in the cooling scenarios of roof and floor (left) and all surfaces (right).

Indoor air movement was caused by buoyancy resulting from the temperature difference between the internal surfaces. Figure 12 presents the roof, wall and floor indoor surface temperatures, to help the understanding of the variation in the air velocity. The case presented was the cooling of the roof and floor with no ventilation and no internal load. The cold floor did not contribute to the air movement in the indoor space, as the dense cold air would stay near the floor. Hence, the velocity was mainly controlled by temperature of walls and roof. The velocity was relatively high during early morning hours due to warm walls and cool roof. The velocity would decline gradually during the morning hours due to a fall in the temperature difference between the walls and the roof. Between 12:00 and 15:00, the velocity was very low as the wall temperature was reduced to below the roof temperature. However, the air velocity did not reach zero due to temperature difference between walls. The air velocity reached a minimum at around 15:00, after which, it rose steadily due to an increase in the temperature difference between wall and roof to reach the maximum at 21:30.

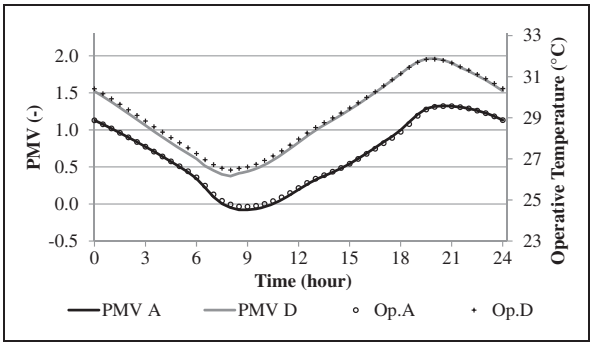

Figure 14. Comparison between the PMV and operative temperature (Op.) in Cases A and D of cooling scenario of roof and floor.

PMV and PPD

In the no cooling scenario, the PMV was higher than 2.7 at all times for all the cases studied. For roof and floor cooling, PMV was in the range of −0.1 to 2, which falls to the range of –1.4 to 0.5 in the scenario of cooling all surfaces. The negative value of PMV indicates that the cooling had exceeded the requirement (Figure 13), which could be avoided by using the control systems. The diurnal trend of PMV was matched closely with that of the operative temperature, as shown in Figure 14. This shows that the operative temperature can give a good indication of the thermal comfort of a conditioned space.

PPD values found in the scenario of no cooling ranged between 97.5 and 100%, indicating that the room was highly uncomfortable. In the cooling of roof and floor scenario, PPD values were improved from 18.5 to 75%, indicating an improvement in indoor comfort. In the cooling of all surfaces scenario, the PPD ranged between 5 and 10.5% (Figure 15). This was after converting all negative PMV values to zero considering the use of the control system to avoid excess cooling.

Conclusions

Passive CCC system supported with CT has been modelled and its performance in terms of indoor air temperature, MRT, air velocity, PMV and PPD was investigated to find the feasibility of adapting this system in hot–semiarid climatic conditions. In summer, the system can provide sufficient cooling for this type of climatic condition. The average PMV was shown to reduce from 3.7 for no cooling to 1.2 for roof and floor cooling. The system's cooling performance was shown to increase when the wall cooling is included in which led to overcooling during morning hours. However, this could be nullified by a suitable control system. PMV value for all surfaces cooling was shown

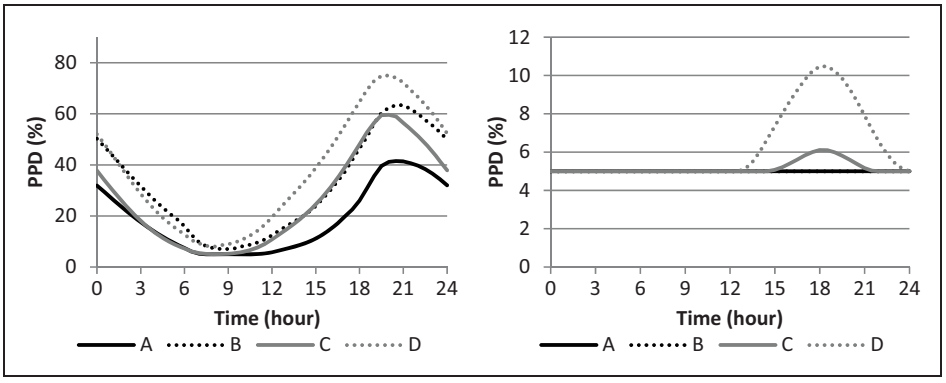

Figure 15. The PPD found in the cooling of roof and floor (left) scenario and cooling of all surfaces (right) scenario.

to be within the range of –0.7 to + 0.5. Further, both CCC system and ventilation were shown to reduce the time lag between temperature extrema of indoor and outdoor air.

Acknowledgment

The authors thank the Indian Institute of Technology Madras, Chennai for providing the facilities.

Authors' contribution

All authors contributed equally in the preparation of this manuscript.

Declaration of conflicting interests

The author(s) declared no potential conflicts of interest with respect to the research, authorship, and/or publication of this article.

Funding

The author(s) disclosed receipt of the following financial support for the research, authorship, and/or publication of this article: The authors thank the Department of Science and Technology, Government of India, New Delhi, for funding this study (Ref.: SR/S3/MERC/00091/2012).

References

1. Global Construction 2025. *Global Construction Perspectives*. 1st ed. London: Oxford Economics, 2013.
2. Population enumeration data (final population), www.censusindia.gov.in (accessed October 7, 2013).
3. Santamouris M and Kolokotsa D. Passive cooling dissipation techniques for buildings and other structures: the state of the art. *Energ Build* 2013; 57: 74–94.
4. *Energy statistics*. 19th issue. New Delhi: Ministry of Statistics and Programme Implementation, 2012..
5. *Industry as a partner for sustainable development: refrigeration*. 1st ed. Uckfield: UNEP, 2002. .
6. Lombard LP, Ortiz J and Pout C. A review on buildings energy consumption information. *Energ Build* 2008; 40: 394–398.
7. Isaac M and Van Vuuren DP. Modeling global residential sector energy demand for heating and air-conditioning in the context of climate change. *Energ Policy* 2009; 37: 507–521.
8. Asimakopoulos DA, Santamouris M, Farrou I, Laskari M, Saliari M, Zanis G, Giannakidis G, Tigas K, Kapsomenakis J, Douvis C, Zerefos SC, Antonakaki T and Giannakopoulos C. Modelling the energy demand projection of the building sector in Greece in the 21st century. *Energ Build* 2012; 49: 488–498.
9. Sekhar SC and Goh SE. Thermal comfort and IAQ characteristics of naturally/mechanically ventilated and air-conditioned bedrooms in a hot and humid climate. *Build Environ* 2011; 46: 1905–1916.
10. Gupta S, Khare M and Goyal R. Sick building syndrome – a case study in a multistory centrally air-conditioned building in the Delhi City. *Build Environ* 2007; 42: 2797–2809.
11. Imanari T, Omori T and Bogaki K. Thermal comfort and energy consumption of the radiant ceiling panel system: comparison with the conventional all-air system. *Energ Build* 1999; 30: 167–175.
12. Brunk MF. Cooling ceilings – an opportunity to reduce energy costs by way of radiant cooling. *ASHRAE Trans* 1993; 99: 479–487.
13. Tian Z and Love JA. A field study of occupant thermal comfort and thermal environments with radiant slab cooling. *Build Environ* 2008; 43: 1658–1670.
14. Olesen BW. Using building mass to heat and cool. *ASHRAE J* 2012; 54: 44–52.
15. Sprecher P and Tillenkamp F. Energy saving systems in building technology based on concrete-core-cooling. *Int J Ambient Energ* 2003; 24: 29–34.
16. Vangtook P and Chirarattananon S. Application of radiant cooling as a passive cooling option in hot humid climate. *Build Environ* 2007; 42: 543–556.
17. Busch JF. A table of two populations: thermal comfort in air conditioned and in naturally ventilated offices in Thailand. *Energ Build* 1992; 18: 235–249.
18. Barnard CL. A theory of fluid flow in compliant tubes. *Biophys J* 1996; 6: 717–724.
19. Lurie MV. *Modeling of oil product and gas pipeline transportation*. 1st ed. Weinheim: WILEY-VCH Verlag GmbH & Co. KGaA, 2008.
20. Gnielinski V. New equation for heat and mass transfer in turbulent pipe and channel flow. *Int Chem Eng* 1976; 16: 359–368.
21. Churchill SW and Bernstein M. A Correlating equation for forced convection from gases and liquids to a circular cylinder in crossflow. *J Heat Trans-T ASME* 1977; 99: 300–307.
22. Weather History, www.wunderground.com (accessed February 23 2015).
23. Sukhatme SP and Nayak JK. *Solar energy: principles of thermal collection and storage*. 3rd ed. New Delhi: Tata McGraw Hill Education Private Limited, 2008.
24. Maiya MP. Analysis of modified counter-flow cooling towers. *Heat Recovery Syst CHP* 1995; 15: 293–303.
25. Stull R. Wet-bulb temperature from relative humidity and air temperature. *J Appl Meteorol Climatol* 2011; 50: 2267–2269.
26. ASHRAE handbook: fundamentals. Atlanta: American Society of Heating, Refrigerating and Air-Conditioning Engineers Inc, 2013..
27. Halawa E, van Hoof J and Soebarto V. The impacts of the thermal radiation field on thermal comfort, energy consumption and control – a critical overview. *Renew Sust Energ Rev* 2014; 37: 907–918.
28. Fanger PO. *Thermal comfort analysis and applications in environmental engineering*. New York: McGraw-Hill, 1970.
29. Fanger PO. *Thermal comfort*. Malabar: Robert E. Krieger, 1982.
30. Stoecker WF and Jones JW. *Refrigeration and air conditioning*. 2nd ed. New Delhi: Tata McGraw Hill, 1982.